Asef controls vascular endothelial permeability and barrier recovery in the lung

Xinyong Tian[a], Yufeng Tian[a], Grzegorz Gawlak[a], Fanyong Meng[a], Yoshihiro Kawasaki[b], Tetsu Akiyama[b], and Anna A. Birukova[a]

[a]Section of Pulmonary and Critical Care Medicine, Department of Medicine, University of Chicago, Chicago, IL 60637; [b]Laboratory of Molecular and Genetic Information, Institute for Molecular and Cellular Biosciences, University of Tokyo, Bunkyo-ku, Tokyo 113-0032, Japan

ABSTRACT **Increased levels of hepatocyte growth factor (HGF) in injured lungs may reflect a compensatory response to diminish acute lung injury (ALI). HGF-induced activation of Rac1 GTPase stimulates endothelial barrier protective mechanisms. This study tested the involvement of Rac-specific guanine nucleotide exchange factor Asef in HGF-induced endothelial cell (EC) cytoskeletal dynamics and barrier protection in vitro and in a two-hit model of ALI. HGF induced membrane translocation of Asef and stimulated Asef Rac1-specific nucleotide exchange activity. Expression of constitutively activated Asef mutant mimicked HGF-induced peripheral actin cytoskeleton enhancement. In contrast, siRNA-induced Asef knockdown or expression of dominant-negative Asef attenuated HGF-induced Rac1 activation evaluated by Rac-GTP pull down and FRET assay with Rac1 biosensor. Molecular inhibition of Asef attenuated HGF-induced peripheral accumulation of cortactin, formation of lamellipodia-like structures, and enhancement of VE-cadherin adherens junctions and compromised HGF-protective effect against thrombin-induced RhoA GTPase activation, Rho-dependent cytoskeleton remodeling, and EC permeability. Intravenous HGF injection attenuated lung inflammation and vascular leak in the two-hit model of ALI induced by excessive mechanical ventilation and thrombin signaling peptide TRAP6. This effect was lost in *Asef*$^{-/-}$ mice. This study shows for the first time the role of Asef in HGF-mediated protection against endothelial hyperpermeability and lung injury.**

Monitoring Editor
Alpha Yap
University of Queensland

Received: Feb 12, 2014
Revised: Dec 4, 2014
Accepted: Dec 11, 2014

INTRODUCTION

The incidence of acute lung injury (ALI) in the United States in 2011 was 129,320 cases/yr (Blank and Napolitano, 2011). Despite protective ventilation strategies, which decreased mortality by ~9%, the remaining 30–40% mortality rate (Acute Respiratory Distress Syndrome Network, 2000) continues to represent a serious threat. Therefore better understanding of the pathological mechanisms driving ALI and equally important intrinsic mechanisms leading to restoration of lung function are needed for development of more efficient therapeutic approaches to ALI.

Clinical studies show dramatic (up to 25-fold) elevation of hepatocyte growth factor (HGF) levels in plasma and bronchoalveolar lavage (BAL) fluid in patients with ALI/acute respiratory distress syndrome (ARDS; Verghese *et al.*, 1998; Stern *et al.*, 2000; Quesnel *et al.*, 2008). In addition to potential involvement in the alveolar epithelial repair process in the lung (Ware and Matthay, 2002), HGF promotes cell survival and enhancement of lung endothelial barrier properties critical for restoration of lung vascular barrier function (Matsumoto and Nakamura, 1996; Liu *et al.*, 2002; Birukova *et al.*, 2007a). These observations suggest that endogenous repair mechanisms, such as HGF elevation, provide essential signals for lung recovery. Our group previously showed HGF-induced activation of Rac1-GTPase, which leads to endothelial barrier protection via

This article was published online ahead of print in MBoC in Press (http://www.molbiolcell.org/cgi/doi/10.1091/mbc.E14-02-0725) on December 17, 2014.

Address correspondence to: Anna Birukova (abirukov@medicine.bsd.uchicago.edu).

Abbreviations used: ALI, acute lung injury; ARDS, acute respiratory distress syndrome; BAL, bronchoalveolar lavage; BSA, bovine serum albumin; CA, constitutively active; CFP, cyan fluorescent protein; DH, Dbl homology; DN, dominant negative; EC, endothelial cell; FRET, fluorescence resonance energy transfer; GEF, guanine nucleotide exchange factor; GFP, green fluorescent protein; HGF, hepatocyte growth factor; HPAEC, human pulmonary artery endothelial cell; HTV, high tidal volume; IL-8, interleukin-8; MLC, myosin light chain; MPO, myeloperoxidase; MYPT1, myosin-associated phosphatase type 1; PBS, phosphate-buffered saline; PBST, PBS-Tween; siRNA, small interfering RNA; TER, transendothelial electrical resistance; TRAP6, thrombin-related activating peptide; VILI, ventilator-induced lung injury; WT, wild type.

enhancement of the peripheral actin cytoskeleton (Liu *et al.*, 2002; Birukova *et al.*, 2007a). However, the upstream mechanism of Rac1 activation by HGF remains unclear.

Rac1 GTPase acts as a molecular switch, cycling between the active, GTP-bound and the inactive, GDP-bound state, and is regulated by guanine nucleotide exchange factors (GEFs) facilitating exchange of GDP for GTP, GTPase-activating proteins (GAPs), which increase the intrinsic rate of GTP hydrolysis by Rac1 GTPase, and guanine nucleotide dissociation inhibitors (RhoGDIs), which associate with inactivated Rac (Boguski and McCormick, 1993; Bishop and Hall, 2000; Zheng, 2001). Rac1 promotes endothelial cell (EC) barrier properties by stimulating peripheral actin polymerization and cortical actin cytoskeletal dynamics, reannealing the disrupted intercellular adherens junctions, forming adherens junction–associated signaling protein complexes, and down-regulating barrier-disruptive Rho GTPase signaling (reviewed in Birukov *et al.*, 2013). Thus molecular mechanisms that precisely control the balance between Rho and Rac1 signaling are essential for EC barrier regulation in physiological and pathological conditions.

Asef is a Rac1-specific GEF that contains a Dbl homology (DH) domain exhibiting GEF activity, a plekstrin homology domain that determines the subcellular localization and activity by interacting with phosphatidylinositol phosphate, an Src homology 3 autoinhibitory domain, and a region that binds tumor suppressor protein APC (APC domain; Kawasaki *et al.*, 2003). Asef has been proposed to regulate the actin cytoskeleton in epithelial and neuronal cells by activating Rac1 and Cdc42 GTPases (Kawasaki *et al.*, 2000). Constitutive Asef activation by truncated APC in colorectal tumor cells caused decreased cell–cell adhesion and aberrant migratory phenotypes (Kawasaki *et al.*, 2013), whereas overexpression of Asef decreased E-cadherin–mediated cell–cell adhesion and promoted migration of kidney epithelial cells (Kawasaki *et al.*, 2003). The role of Asef in vascular endothelial barrier regulation is unknown.

This study used several complementary approaches, including biochemical assays, live imaging, and molecular inhibition to investigate the role of Asef in control of lung endothelial barrier and HGF-induced vascular barrier protection. Using a genetic animal model, we evaluated the role of Asef in the two-hit animal model of acute lung injury. Asef-dependent mechanisms of Rac1 activation and HGF-induced endothelial barrier protection were linked to the down-regulation of the barrier-disruptive Rho pathway.

RESULTS

HGF-induced activation of Asef triggers Rac1 signaling

The HGF-induced endothelial barrier protective response is associated with activation of Rac1 GTPase signaling, but the precise mechanisms of Rac1 activation remain elusive. We found that HGF induced activation of Rac1 (Figure 1A), which was associated with rapid stimulation of Asef nucleotide exchange activity toward Rac1 observed at 2–10 min after HGF addition (Figure 1B). Western blot analysis showed comparable levels of Asef expression in both human lung microvascular and pulmonary artery EC cultures. These data suggest the role for Asef-dependent signaling mechanisms in ECs from different vascular beds. HGF-induced activation of Asef guanine nucleotide exchange activity toward Rac1 was abrogated by cell pretreatment with the pharmacological inhibitor of HGF receptor c-Met (Figure 1C). Activation of Asef by HGF also led to Asef translocation to the cell membrane fraction (Figure 1D), with preferential accumulation at the cell periphery as visualized by immunofluorescence staining with Asef antibody (Figure 1E).

Molecular inhibition of Asef in pulmonary ECs using small interfering RNA (siRNA)–mediated knockdown delayed establishment of endothelial monolayers as monitored by measurements of transendothelial electrical resistance (TER; Figure 2A). Using the Rac1 fluorescence resonance energy transfer (FRET) biosensor (Birukova *et al.*, 2012), we evaluated the time course of regional Rac1 activation in subconfluent pulmonary EC cultures. HGF induced rapid activation of Rac1 (Figure 2B), whereas Asef knockdown significantly suppressed HGF-induced Rac1 activation. The quantitative analysis of FRET data is summarized in Figure 2C. Because this study investigated the ability of HGF to restore endothelial monolayer integrity, the subconfluent EC cultures were used in the following experiments. Asef knockdown abolished HGF-induced Rac1 activation, monitored by Rac-GTP pull-down assay (Figure 2D). To test whether Asef-mediated Rac1 activation is additionally regulated by cell–cell contacts, we also evaluated HGF-induced Rac1 activity in sparse (Figure 2E) and dense (confluent; Figure 2F) EC cultures. Representative phase-contrast microscopy images in Figures 2, D–F, depict cell density of human pulmonary artery endothelial cell (HPAEC) cultures used in these experiments, although actual densities could slightly vary between experiments. HGF activated Rac1 GTPase at all three cell density conditions, and the effect was abolished by Asef knockdown.

Asef mediates dynamic peripheral cytoskeletal remodeling in HGF-stimulated EC

Several actin-binding proteins, including the Arp2/3 complex, p21Arc, PAK1, and cortactin, control peripheral actin polymerization and cortical actin structure (Borisy and Svitkina, 2000; Weed and Parsons, 2001). Cortactin is an actin-binding activator of peripheral actin polymerization (Uruno *et al.*, 2001). Translocation of cortactin to the cell periphery is mediated by Rac1 and blocked in cells with inhibited Rac1 activity (Weed *et al.*, 1998). Rac1 activation is also required for cortactin tyrosine phosphorylation and activation of actin cytoskeletal dynamics such as membrane ruffling and lamellipodia formation (Vouret-Craviari *et al.*, 2002; Head *et al.*, 2003; Ammer and Weed, 2008). Involvement of Asef in HGF-induced peripheral cytoskeletal dynamics was first evaluated by analysis of cortactin membrane translocation, which indicates cortactin activation (Uruno *et al.*, 2001; Dudek *et al.*, 2004). HGF stimulated cortactin translocation to the membrane fraction; this effect was attenuated by Asef knockdown (Figure 3A). Rac1 activation triggers signaling pathways leading to increased cortactin tyrosine phosphorylation (Head *et al.*, 2003). Indeed, we observed HGF-induced increase in cortactin phosphorylation at Tyr-421, which was markedly attenuated by Asef knockdown (Figure 3B).

The Asef-dependent mechanism of HGF-induced activation of peripheral actin cytoskeletal dynamics was further examined in experiments with live imaging of green fluorescent protein (GFP)–tagged cortactin. HGF induced rapid formation of cortactin-positive lamellipodia-like structures, which were observed as early as 2 min and remained prominent during the 30-min observation period (Figure 3C, top). In contrast, Asef knockdown abolished HGF-induced activation of peripheral cytoskeletal remodeling (Figure 3C, bottom). Insets in Figure 3C depict phase-contrast microscopy images of tested cells. Collectively these results demonstrate a critical role of Asef in the activation of cortical cytoskeletal dynamics via stimulation of Rac1 cytoskeletal effectors.

Potential effect of EC confluence on Asef-dependent peripheral cortactin activation and actin cytoskeletal remodeling was further tested. Activation of cortactin in response to HGF was reflected by cortactin phosphorylation and accumulation in cell-peripheral lamellipodia-like structures and was observed in both sparse and dense EC monolayers (Figure 3, D and E). These effects were markedly attenuated by Asef knockdown in both sparse and dense EC cultures.

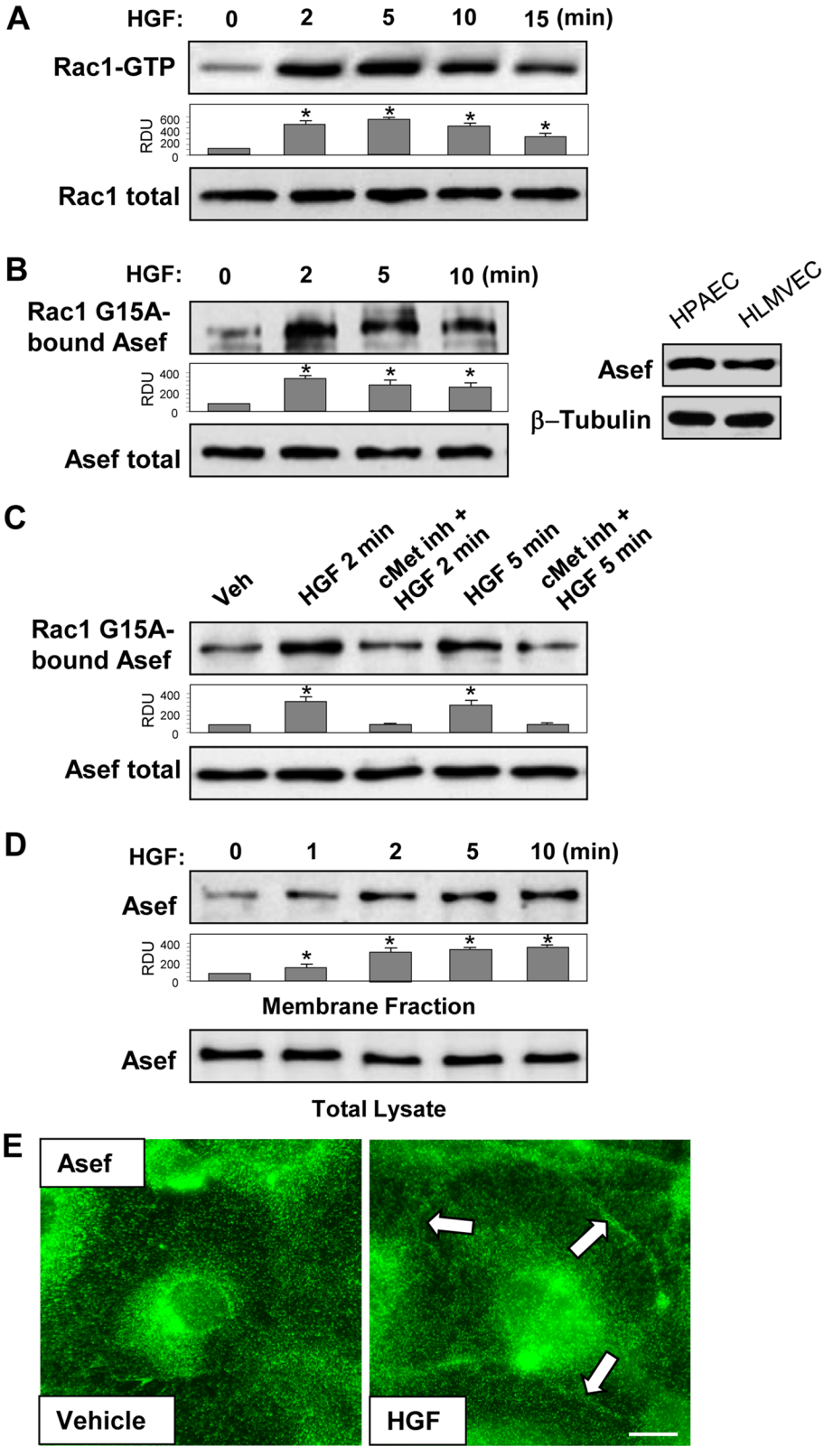

FIGURE 1: HGF induces activation of Asef and Rac1. (A–D) HPAECs were stimulated with HGF (50 ng/ml) for the indicated periods of time. (A) Rac1 activation was determined by Rac-GTP pull-down assay. Content of activated Rac1 was normalized to the total Rac1 content in EC lysates. *$p < 0.05$ vs. vehicle. (B) Asef activation was determined by pull-down assay with immobilized Rac1G15A and evaluated by increased Asef association with Rac1G15A. Content of activated Asef was normalized to the total Asef content in EC lysates. *$p < 0.05$ vs. vehicle. (C) HPAECs were preincubated with vehicle or c-Met inhibitor (carboxamide 50 nM, 30 min), followed by stimulation with HGF (2 and 5 min). Asef activation was determined by pull-down assay with immobilized Rac1G15A and normalized to the total Asef. *$p < 0.05$ vs. cMet inh + HGF. (D) HPAECs were stimulated with HGF, followed by isolation of cytosolic and membrane fractions. Time-dependent, HGF-induced accumulation of Asef in membrane fraction was detected with specific antibodies. Asef content in corresponding total cell lysates was used as a normalization control. *$p < 0.05$ vs. vehicle. (E) Endothelial cells grown on glass coverslips were stimulated with HGF (50 ng/ml, 30 min). Intracellular redistribution of endogenous Asef was examined by immunofluorescence staining with Asef antibody. Representative results of three to five independent experiments. Bar, 5 μm.

Cortactin translocation was also accompanied by increased F-actin accumulation at cell peripheral compartments (Figure 4A). Inspection of subcortical F-actin accumulation at different cell regions revealed that HGF-induced cortical F-actin accumulation in lamellipodia-like structures was observed in regions with intercellular gaps (inset 1 in Figure 4A) but also in the regions of established cell–cell contacts (inset 2 in Figure 4, A and B). HGF-induced cortical actin dynamics was inhibited by Asef knockdown (Figure 4, A and B). These data show that HGF-induced Asef activity stimulates cortical cytoskeletal dynamics in a cell contact–independent manner.

Asef mediates HGF-induced endothelial barrier enhancement

The role of Asef in HGF-induced EC barrier enhancement was further investigated in functional tests using measurements of TER. Confluent human pulmonary ECs grown on the gold microelectrodes for TER measurements were transfected with Asef-specific siRNA duplexes. Control cells were transfected with nonspecific RNA. The basal TER levels were not affected by Asef knockdown (unpublished data). Asef depletion significantly attenuated HGF-induced EC barrier enhancement as monitored by reduced TER increase in a dose-dependent manner (Figure 4C).

The effects of Asef knockdown on HGF-induced EC barrier enhancement were further tested using visualization of local areas in EC monolayers with increased EC permeability for macromolecules (Figure 4D). In control conditions, some accumulation of fluorescein isothiocyanate (FITC)–labeled tracer at sites underlying the cell–cell junction area was observed. These results reflect the basal level of mass transport across the cell–cell junction area in EC monolayers. HGF significantly decreased the basal EC

monolayer permeability for FITC-labeled avidin (Figure 4D, bottom left). The barrier-enhancing effect of HGF was abrogated in EC monolayers with Asef knockdown (Figure 4D, bottom right).

Modulation of Asef activity affects HGF-induced peripheral cytoskeletal enhancement

As a complementary approach to experiments with Asef knockdown, we performed ectopic expression of HA-tagged wild-type Asef or its constitutively activated (CA-Asef) or dominant-negative (DN-Asef) mutant (Kawasaki *et al.*, 2003). Overexpression of wild-type Asef further enhanced EC peripheral actin remodeling in response to HGF in comparison to HGF-stimulated nontransfected cells (Figure 5A). In turn, expression of activated Asef mutant in nonstimulated cells reproduced peripheral actin cytoskeletal rearrangement observed in nontransfected ECs treated with HGF (Figure 5B). Similar to Asef knockdown experiments, the expression of dominant-negative Asef abrogated HGF-induced formation of lamellipodia-like structures and peripheral actin rim (Figure 5C). Expression of dominant-negative Asef mutant suppressed the HGF-induced activation of Rac1 GTPase in pulmonary ECs (Figure 5D).

Adherens junction formation in HGF-stimulated HPAEC is cell density dependent and controlled by Asef

VE-cadherin accumulation at the cell membrane compartment is essential for initiation adherens junction protein complex assembly. Using subcellular fractionation assay, we examined VE-cadherin membrane translocation in confluent (Figure 6A) and sparse (Figure 6B) EC cultures after HGF stimulation. HGF induced robust VE-cadherin membrane accumulation in dense (confluent) EC monolayers but not in sparse EC cultures. Observed VE-cadherin membrane accumulation was significantly attenuated in HGF-stimulated ECs with Asef knockdown. Immunofluorescence staining of VE-cadherin shows a dramatic increase of VE-cadherin–positive immunofluorescence signal at the cell junction area of HGF-stimulated EC monolayers. This effect was abolished by Asef knockdown (Figure 6C).

Next we tested the role of Asef in regulation of interaction between VE-cadherin and its adherens junction binding partner, p120-catenin. HPAECs with depleted Asef or control cells were stimulated with HGF, and VE-cadherin–p120-catenin interactions were tested by reciprocal coimmunoprecipitation assays using VE-cadherin or p120-catenin antibodies. HGF treatment of control ECs further increased interaction between VE-cadherin and p120-catein, which was suppressed in Asef-depleted cells (Figure 6D). These data suggest an Asef-dependent mechanism of HGF-induced assembly of VE-cadherin adherens junction protein complex and link these effects with EC barrier enhancement.

Asef mediates protective effect of HGF against thrombin-induced EC permeability

Agonist-induced activation of Rac1 protects the vascular endothelial barrier in thrombin-stimulated ECs by inhibiting the thrombin-induced Rho pathway of barrier dysfunction (Finigan *et al.*, 2005; Birukova *et al.*, 2007c; Tauseef *et al.*, 2008; Baumer *et al.*, 2009). Involvement of Asef in HGF-induced barrier protective effects against thrombin was tested in control and Asef-depleted cells. Agonist-induced permeability responses in control cells treated with nonspecific RNA and Asef-depleted EC monolayers were monitored by TER measurements. HGF exhibited a prominent protective effect against thrombin-induced TER decline in EC monolayers treated with nonspecific RNA (Figure 7A, left). In contrast, Asef knockdown impaired HGF-induced EC barrier protection against thrombin (Figure 7A, right). Effects of Asef knockdown on agonist-induced TER changes are summarized in the bar graph in Figure 7A (bottom).

The role of Asef in the HGF-induced preservation of EC monolayer integrity was further examined by immunofluorescence studies. Control and Asef-depleted EC were challenged with thrombin with or without HGF pretreatment. Thrombin induced rapid formation of stress fibers and intercellular gaps, which was observed in both control and Asef-depleted EC monolayers (Figure 7B). HGF partially preserved the integrity of thrombin-challenged EC monolayers treated with nonspecific RNA, but this protective effect was lost in ECs with depleted Asef.

The Rho pathway of endothelial permeability involves phosphorylation of myosin-binding subunit of myosin-associated phosphatase type 1 (MYPT1) at the Rho kinase–specific site Thr-850 (Essler *et al.*, 1998; Velasco *et al.*, 2002), leading to increased myosin light chain (MLC) phosphorylation and activated actomyosin contraction. We examined effects of HGF and thrombin on Rho activation (Figure 7C) and MYPT1 and MLC phosphorylation levels (Figure 7D) in control and Asef-depleted cells. Thrombin stimulation strongly activated Rho and increased MYPT1 and MLC phosphorylation in both control cells and cells with Asef knockdown. However, attenuation of thrombin-induced Rho signaling by HGF pretreatment was observed in control HGF- and thrombin-treated ECs but not in ECs with Asef knockdown.

Asef mediates protective effects of HGF in the two-hit model of lung injury

The foregoing studies in pulmonary EC culture demonstrate a critical role for Asef as a key mediator of HGF-induced Rac1 signaling leading to activation of peripheral actin cytoskeletal dynamics and endothelial barrier enhancement, as well as attenuation of Rho-dependent barrier- disruptive mechanisms. Development of ventilator-induced lung injury (VILI) is a complex process triggered by pathological mechanical forces acting on lung tissue and accompanied by elevation of circulating proinflammatory cytokines and mediators (interleukin-8 [IL-8], IL-1β, coagulation proteins, etc.). Based on these findings, a two-hit (or even multiple-hit) animal model of VILI has been accepted to better represent the clinical manifestations of acute lung injury (Matthay *et al.*, 2003). The role of Asef in the vascular protective effects of HGF was further investigated in the two-hit model of lung injury previously characterized by our group (Birukova *et al.*, 2010, 2011), which was induced by mechanical ventilation at high tidal volume (HTV; 30 ml/kg) combined with intravenous injection of thrombin-related activating peptide (TRAP6), the thrombin-derived nonthrombogenic peptide that serves as a PAR1-receptor ligand (Storck and Zimmermann, 1996).

Asef$^{-/-}$ mice and matching *Asef*$^{+/+}$ controls were injected with vehicle or HGF before challenge with TRAP6 and mechanical ventilation. Evaluation of the BAL after 4 h of TRAP6/HTV revealed a significant elevation of BAL protein content, reflecting lung barrier dysfunction in both *Asef*$^{+/+}$ and *Asef*$^{-/-}$ mice (Figure 8A). However, HGF-protective effects against TRAP6/HTV-induced increases in BAL protein content observed in *Asef*$^{+/+}$ controls were abolished in *Asef*$^{-/-}$ mice. TRAP6/HTV-induced lung injury caused significant lung vascular leak detected by Evans blue dye accumulation in the lung parenchyma, which was evident in *Asef*$^{+/+}$ and *Asef*$^{-/-}$ mice after 4 h of HTV. In turn, pretreatment with HGF caused a substantial decrease in Evans blue accumulation in *Asef*$^{+/+}$ but not *Asef*$^{-/-}$ mice. Images of original lung preparations showing Evans blue extravasation are shown in Figure 8B. Quantitative analysis of Evans blue–labeled albumin in the lung tissue extracts from these experiments is presented in Figure 8C.

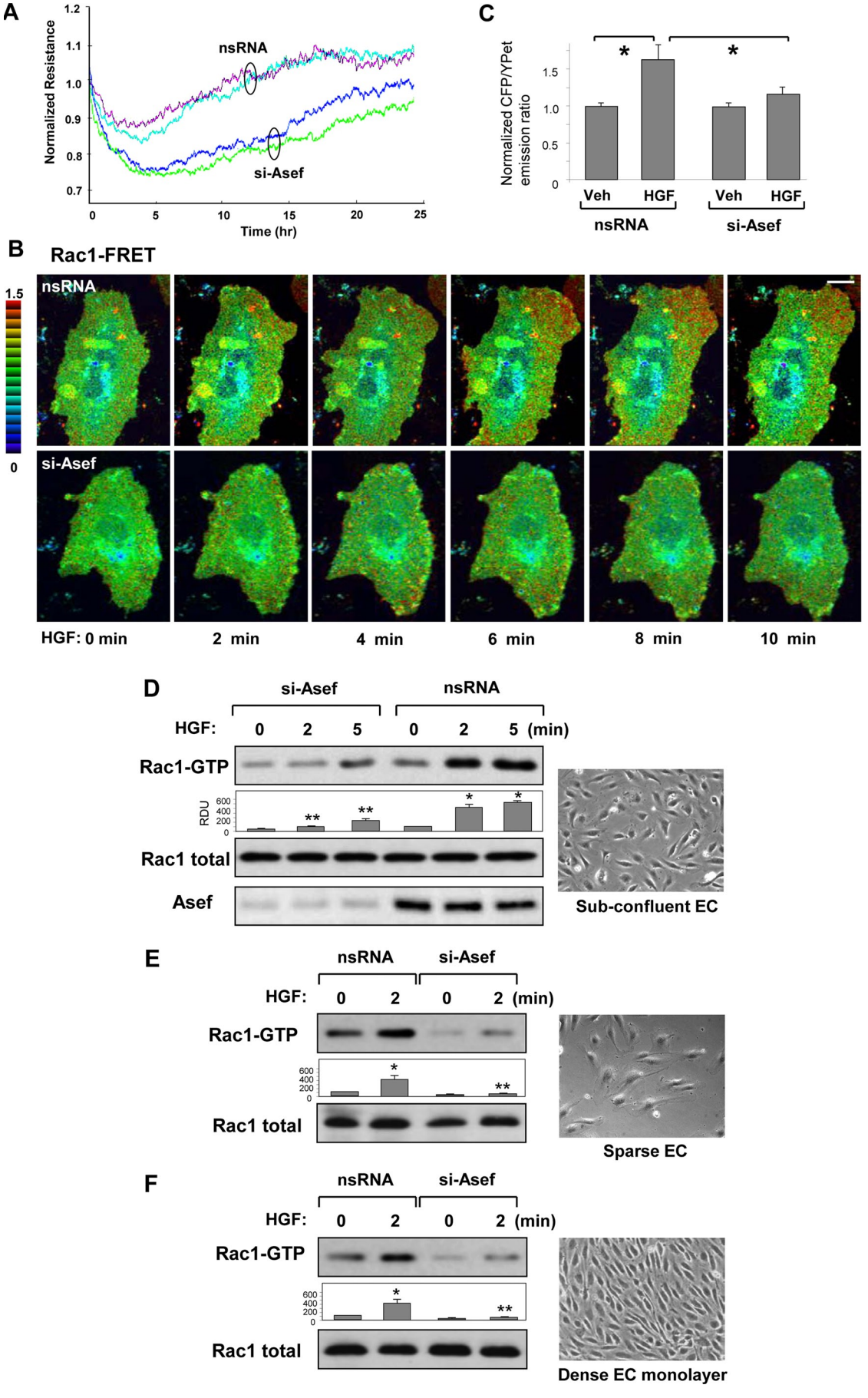
A
Normalized Resistance
nsRNA
si-Asef
Time (hr)
C
Normalized CFP/YPet emission ratio
Veh
HGF
nsRNA
si-Asef
B
Rac1-FRET
nsRNA
si-Asef
HGF: 0 min
2 min
4 min
6 min
8 min
10 min
D
si-Asef
nsRNA
HGF:
Rac1-GTP
RDU
Rac1 total
Asef
Sub-confluent EC
E
nsRNA
si-Asef
HGF:
Rac1-GTP
Rac1 total
Sparse EC
F
nsRNA
si-Asef
HGF:
Rac1-GTP
Rac1 total
Dense EC monolayer

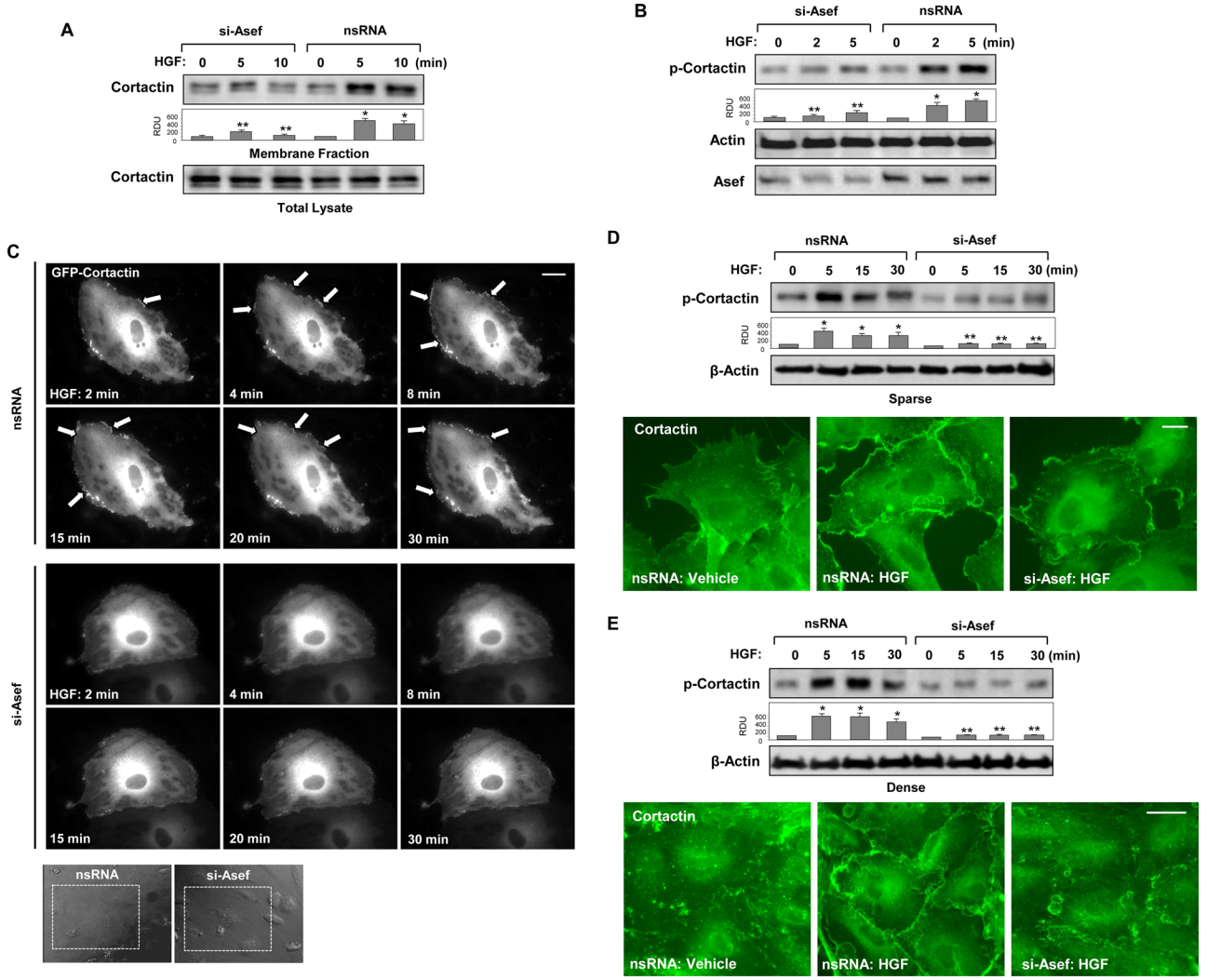

FIGURE 3: Asef knockdown attenuates HGF-induced cortactin activation. HPAECs were transfected with Asef-specific siRNA or nonspecific RNA and stimulated with HGF (50 ng/ml). (A) After isolation of cytosolic and membrane fractions, cortactin accumulation in membrane fraction was monitored by Western blot. Cortactin content in corresponding total cell lysates was used as a normalization control. (B) Effect of Asef knockdown on HGF-induced cortactin phosphorylation was evaluated by Western blot with phospho–Tyr-421-cortactin antibody. Equal protein loading was confirmed by membrane probing with β-actin antibody. siRNA-induced Asef protein depletion was confirmed by Western blot analysis of whole-cell lysates. *$p < 0.01$ vs. nonstimulated cells treated with nonspecific RNA; **$p < 0.01$ vs. nonspecific RNA. (C) Live-cell imaging of HPAECs transfected with Asef siRNA or nonspecific RNA and expressing GFP-cortactin. Snapshots depict HGF-induced cortical dynamics at cell periphery of control and Asef-depleted cells. Bar, 5 μm. (D, E) Effect of Asef knockdown on HGF-induced cortactin phosphorylation in sparse (D; bar, 5 μm) or dense (E; bar, 10 μm) HPAEC culture was evaluated by Western blot with phospho–Tyr-421-cortactin antibody. Equal protein loading was confirmed by membrane probing with β-actin antibody. *p <0.01 vs. nonstimulated cells treated with nonspecific RNA; **$p < 0.01$ vs. nonspecific RNA. HGF-induced cortactin translocation was evaluated by immunofluorescence staining of formaldehyde-fixed ECs. Results are representative of three independent experiments.

FIGURE 2: Asef knockdown attenuates HGF-induced Rac1 activation. (A) Endothelial cells were transfected with control or 100 nM Asef-specific siRNA, and after 24 h, changes in TER were monitored over time. (B) FRET analysis of HGF-induced Rac1 activation. HPAECs were transfected with nonspecific or Asef-specific siRNA duplexes for 24 h, followed by transfection with CFP/YPet-Rac1 biosensor for an additional 24 h. FRET analysis of time-dependent Rac activation was performed in HGF-stimulated control and Asef-knockdown cells. Images represent a ratio of activated Rac1 to the total Rac1 content. Areas of Rac1 activation appear in red. Bar, 5 μm. (C) Quantitative analysis of HGF-induced Rac1 activation at the cell periphery. Bar graphs represent normalized CFP/YPet emission ratio. Rac1 activation in cells before HGF stimulation was compared with Rac1 activation after 6 min of HGF addition. Data are expressed as mean ± SD of four independent experiments, five to seven cells for each experiment; *$p < 0.05$. (D–F) Subconfluent (D), sparse (E), or dense (F) HPAECs were transfected with Asef-specific siRNA or nonspecific RNA and stimulated with HGF (50 ng/ml). Left, Rac1 activation determined by Rac-GTP pull-down assay. The content of activated Rac1 was normalized to the total Rac1 content in EC lysates. *p <0.01 vs. nonstimulated cells treated with nonspecific (ns) RNA; **p <0.01 vs. nsRNA. Right, representative phase-contrast images of HPAECs used for experiments.

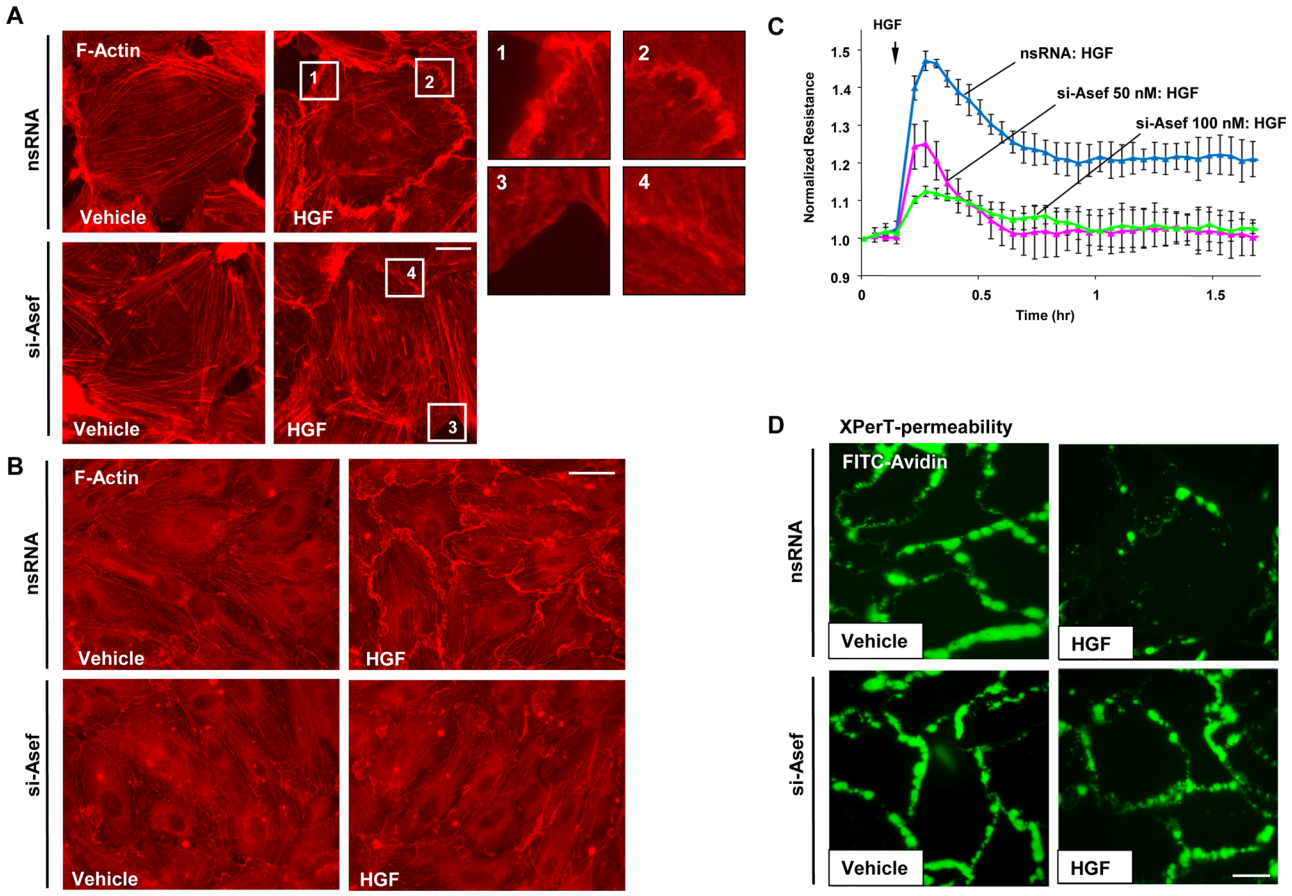

FIGURE 4: Asef knockdown attenuates HGF-induced peripheral actin remodeling and EC barrier enhancement. (A, B) Control and Asef-depleted EC were stimulated with HGF (50 ng/ml, 10 min). Immunofluorescence visualization of actin cytoskeleton was performed in subconfluent (A; bar; 5 μm) or dense (B; bar, 10 μm) EC culture using TR-phalloidin staining. HGF-induced peripheral accumulation of polymerized actin was abolished by Asef knockdown. Magnified images (insets) show details of actin structure. (C) Permeability measurements. Control and Asef-depleted ECs were stimulated with HGF (50 ng/ml), and TER was monitored over time. Cumulative data of five independent experiments. Results are represented as mean ± SD. (D) HPAECs grown on glass coverslips with immobilized biotinylated gelatin (0.25 mg/ml) and transfected with Asef-specific siRNA or nonspecific RNA and then stimulated with vehicle or HGF (50 ng/ml, 10 min), followed by addition of FITC-avidin (25 μg/ml, 3 min). Unbound FITC-avidin was removed, and FITC fluorescence signal was visualized by fluorescence microscopy. Bar, 10 μm.

Exposure to TRAP6/HTV also significantly increased the total cell and neutrophil count in BAL samples in both *Asef*$^{+/+}$ and *Asef*$^{-/-}$ mice as compared with the nonventilated controls (Figure 9A). Although we observed a trend toward higher levels of BAL cell count in TRAP6/HTV-treated *Asef*$^{-/-}$ mice, it did not reach statistical significance. By contrast, HGF administration before TRAP6/HTV caused significant reduction of cellular infiltration in *Asef*$^{+/+}$ but not *Asef*$^{-/-}$ mice. TRAP6/HTV caused a significant increase in lung myeloperoxidase (MPO) activity compared with the control group (Figure 9B). HGF decreased MPO activity in the lungs of TRAP6/HTV-exposed *Asef*$^{+/+}$ mice, whereas in *Asef*$^{-/-}$ mice, this effect was statistically insignificant.

Histological analysis of lung sections showed that TRAP6/HTV induced inflammatory cell infiltration (predominantly neutrophils and mononuclear cells) in both lung interstitium and alveolar compartments of *Asef*$^{+/+}$ and *Asef*$^{-/-}$ mice (Figure 9C). Pretreatment with HGF markedly attenuated TRAP6/HTV-induced inflammatory cell infiltration in lung tissue of *Asef*$^{+/+}$ mice but failed to induce comparable protective effects in *Asef*$^{-/-}$ mice.

DISCUSSION

Alterations in vascular permeability are the defining feature of diverse processes, including inflammation, ischemia/reperfusion, and ventilator-induced lung injury. Increased endothelial permeability causes alveolar flooding, hypoxemia, and tissue leukocyte infiltration, which triggers inflammatory cytokine production and may lead to increased morbidity and mortality. Increased levels of circulating HGF have been observed in experimental models and in patients with acute lung injury and ARDS syndrome (Ware and Matthay, 2002; Geiser, 2003). Of importance, HGF up-regulation by pathogenic stimuli has been linked to pulmonary recovery after pathological insult (Ware and Matthay, 2002; Geiser, 2003), suggesting that HGF may serve as a protective agonist in lung-reparative processes and in restoration of vascular permeability to normal levels. However, the molecular mechanisms of the underlying effects of HGF on pulmonary EC barrier restoration are not yet well understood.

This study shows for first time the role of Asef in the HGF-induced establishment of EC monolayer integrity and Asef-dependent regulation of agonist-induced vascular endothelial permeability.

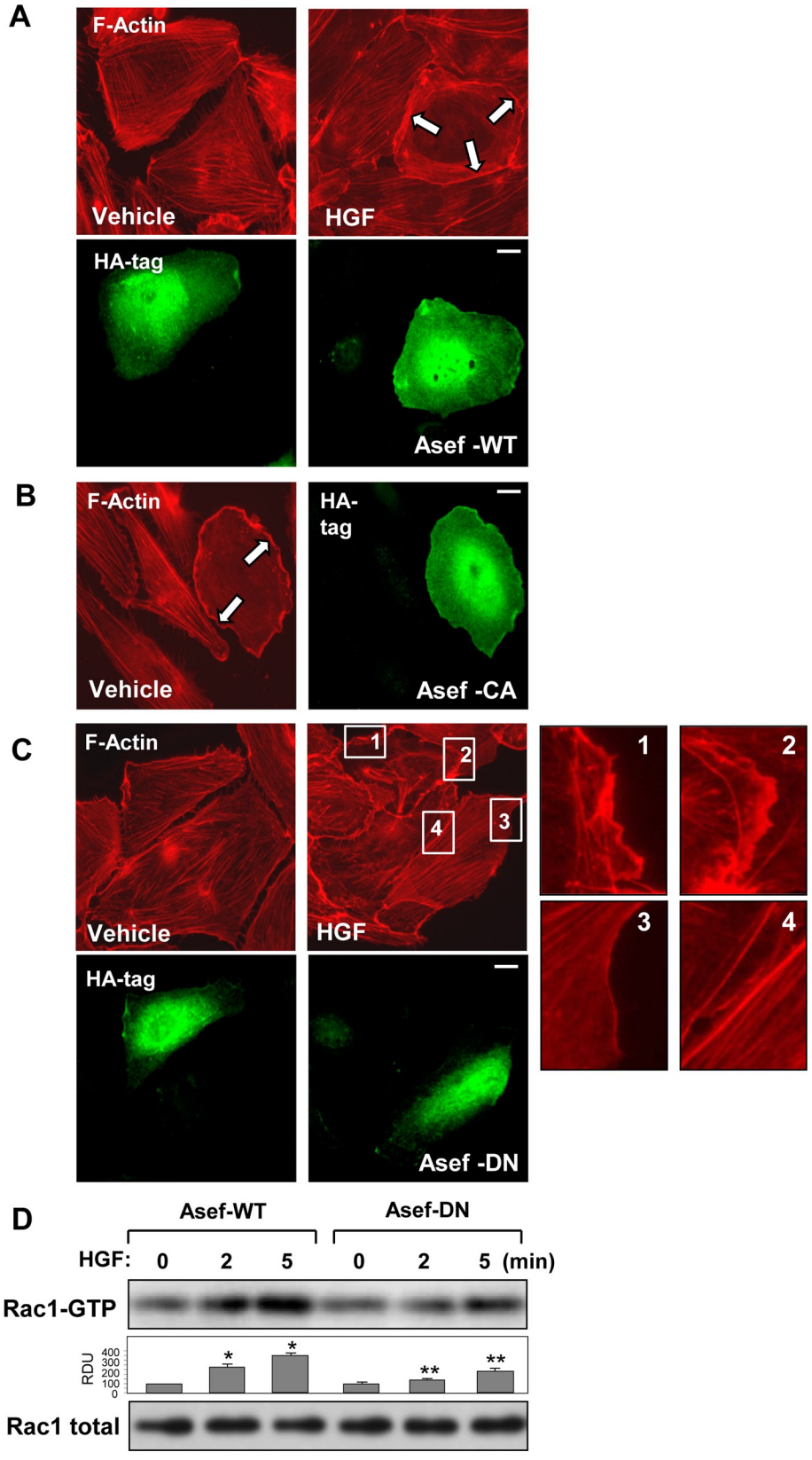

FIGURE 5: Role of Asef activity in HGF-induced actin remodeling. HA-tagged wild-type Asef, constitutively active (CA-Asef) or dominant-negative (DN-Asef) Asef mutants were expressed in HPAECs. After stimulation with vehicle or HGF (50 ng/ml, 10 min), cells were fixed in 4.7% formaldehyde, and F-actin was visualized by Texas red–phalloidin staining. Cells expressing recombinant Asef were visualized by immunofluorescence staining for HA tag. (A) Cells transfected with wild-type (WT) Asef were treated with vehicle or HGF. (B) Expression of constitutively active Asef mutant (ΔAPC-Asef). (C) Expression of dominant-negative Asef mutant (ΔDH-Asef). Inset, higher-magnification image of cell edge, depicting inhibition of HGF-induced formation of lamellipodia-like structures by expression of dominant-negative Asef mutant. Arrows show cells with activated peripheral actin cytoskeletal remodeling. Bar, 5 μm. (D) EC monolayers were transiently transfected with wild-type Asef or dominant-negative Asef mutant, and HGF-induced Rac1 activation was determined by Rac-GTP pull-down assay. The content of activated Rac1 was normalized to the total Rac1 content in EC lysates; *$p < 0.01$ vs. nonstimulated controls transfected with Asef-WT; **$p < 0.05$ vs. Asef-WT.

HGF-induced Asef activation triggered activation of Rac1 and stimulated peripheral actin cytoskeletal dynamics in the pulmonary endothelium, which is a key mechanism of endothelial integrity restoration. Peripheral localization of Asef in the HGF-stimulated cells suggested that local activation of Rac1 signaling is also critical for reestablishment of cell–cell junction complexes (Noren *et al.*, 2001; Arthur *et al.*, 2002; Birukova *et al.*, 2012) and further enhancement of the EC barrier.

To further elucidate these mechanisms, we performed additional studies in sparse, subconfluent, and confluent EC cultures exposed to HGF. The results show that cell seeding density and cell contact state did not impair Asef-mediated Rac1 signaling and activation of cortical actin cytoskeletal dynamics induced by HGF. Of interest, the data showed that Asef mediates HGF-induced formation of lamellipodia-like structures even in confluent EC monolayers with established cell–cell junctions. In contrast, HGF-induced, Asef-dependent VE-cadherin membrane translocation and VE-cadherin association with p120-catenin were detected in confluent EC monolayers but not in sparse EC cultures. These results suggest that HGF-induced establishment of EC intercellular junctions is mediated by Asef but requires cell contacts formed by HGF-stimulated expanding cells. Taken together, these data provide compelling evidence for Asef's role in the HGF-induced reestablishment of EC monolayer integrity and barrier properties via two complementary mechanisms: activation of peripheral actin cytoskeletal dynamics, leading to cell extension and closing of gaps in a monolayer, and formation of cell–cell contacts, in which Asef stimulates establishment of specialized junctional structures.

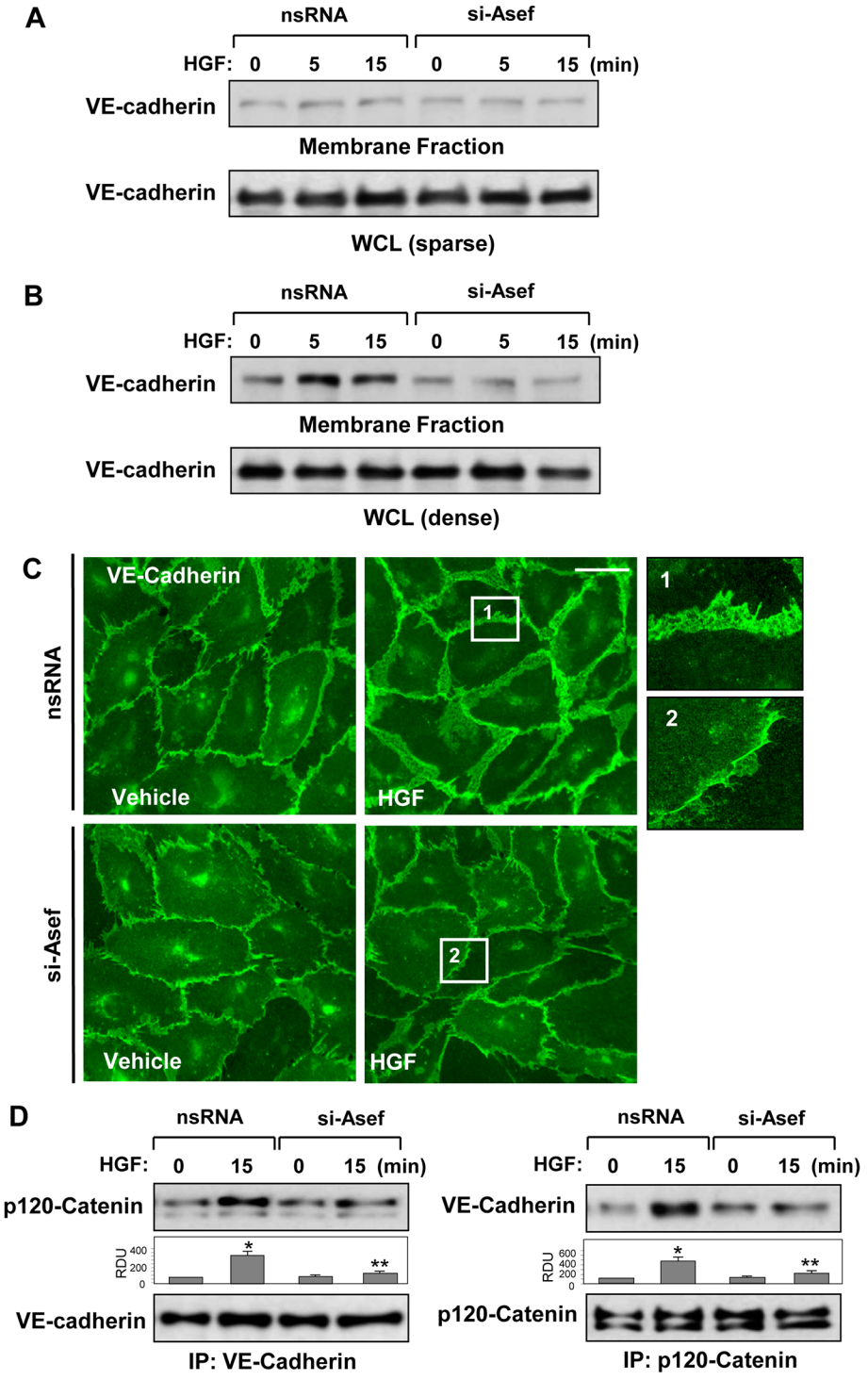

FIGURE 6: Asef knockdown attenuates HGF-induced enhancement of adherens junctions. HPAECs were transfected with Asef-specific siRNA or nonspecific RNA and stimulated with HGF (50 ng/ml). Sparse (A) or dense (B) HPAEC cultures were stimulated with HGF, followed by isolation of membrane fraction. HGF-induced VE-cadherin accumulation in the membrane fraction was detected with specific antibodies. VE-cadherin content in corresponding total cell lysates was used as a normalization control. (C) Visualization of cell–cell contacts was performed by immunofluorescence staining of formaldehyde-fixed HPAECs with VE-cadherin antibody. Bar, 10 μm. Magnified images (insets) show details of adherens junction structures. (D) HGF-treated HPAECs were used for reciprocal coimmunoprecipitation assays with VE-cadherin (top) and p120-catenin (bottom) antibodies, followed by Western blot detection of p120-catenin and VE-cadherin; *p <0.01 vs. nonstimulated cells treated with nonspecific RNA; **p <0.05 vs. nonspecific RNA. Results are representative of three independent experiments.

Restoration of EC integrity and cell junctions also requires local down-regulation of Rho signaling (Anastasiadis *et al.*, 2000). Our previous studies described the mechanism of local Rho inhibition via Rac1-mediated activation of the Rho-specific negative regulator p190RhoGAP and its recruitment to adherens junctions by p120-catenin (Birukova *et al.*, 2011; Zebda *et al.*, 2013), leading to enhancement of cortical actin, disappearance of central stress fibers, and EC barrier enhancement. Dissolution of central stress fibers due to Rho inactivation and activation of cortical actin remodeling and cell junctions in endothelial cells stimulated with Rac1-activating agonists is well recognized (Garcia *et al.*, 2001; Birukov *et al.*, 2004; Dudek *et al.*, 2004; Fukuhara *et al.*, 2005), and the p190RhoGAP-dependent Rho inactivation discussed earlier is one of several potential mechanisms of HGF-induced suppression of Rho activity. Other mechanisms of negative Rho regulation by HGF-induced Rac1 signaling may include direct interaction of Rac1 with Rho inhibitor RhoGDI (Stultiens *et al.*, 2012), inhibition of the low–molecular weight protein tyrosine phosphatase, leading to activation of p190RhoGAP (Nimnual *et al.*, 2003), and down-regulation of Rho-specific guanine nucleotide exchange factors resulting in reduction of the RhoGTP pool. For example, a recent study described HGF-induced microtubule growth (Tian *et al.*, 2014), which may lead to capture and inactivation of MT-interacting, Rho-specific GEF-H1. Detailed mechanisms of Asef-dependent Rac1-Rho cross-talk in HGF-stimulated endothelium await further investigation. It is also possible that HGF-induced activation and accumulation of Asef at the cell junction area observed in this study promotes EC barrier restoration by triggering Rac1-dependent recruitment to the cell periphery and activation of p190RhoGAP. This intriguing possibility warrants further investigation.

In addition to the Asef described in this study, another Rac1-specific GEF, Tiam1, was also implicated in HGF-protective effects (Birukova *et al.*, 2007a; Singleton *et al.*, 2007). Nucleotide exchange activity of Tiam1, which mediates HGF-induced Rac1 activation and EC barrier protective response, can be regulated by diverse mechanisms, including phosphorylation by tyrosine kinases, Ca^{2+}/calmodulin–dependent kinase II, or related kinases, interaction with the phosphoinositide 3-kinase product phosphatidylinositol (3,4,5)-trisphosphate, and binding to the cell surface molecule CD44 or cytoskeletal protein ankyrin, as well as direct binding to activated Ras

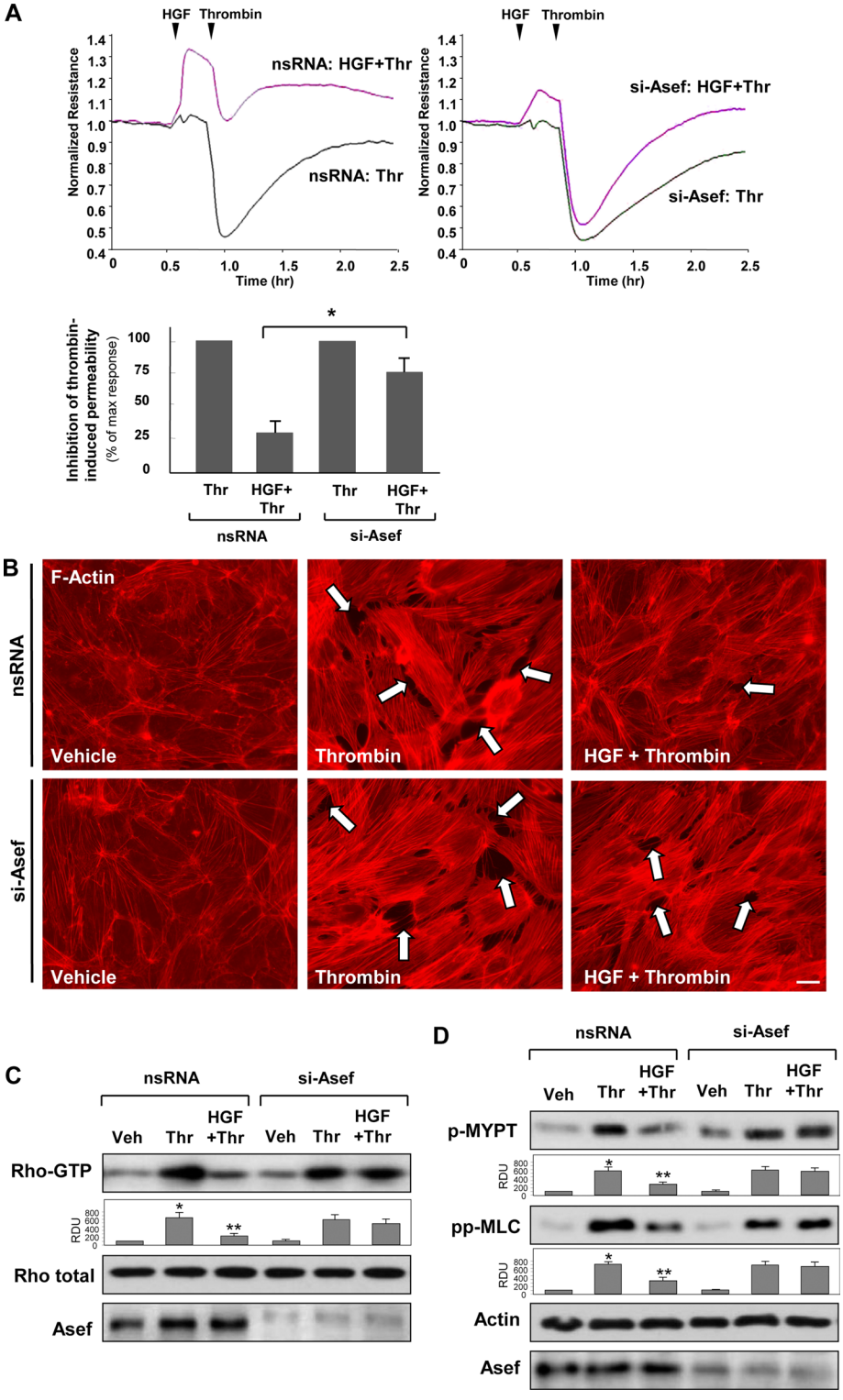

FIGURE 7: Asef knockdown attenuates HGF protective effects against thrombin-induced EC barrier disruption. (A) Measurements of TER. ECs were transfected with 100 nM Asef-specific siRNA or nonspecific RNA 72 h before TER measurement. After 15-min pretreatment with vehicle or HGF, cells were stimulated with thrombin (0.5 U/ml; arrow). The TER was monitored over time. Representative data of five independent experiments. Bar graph depicts EC permeability changes at the time point corresponding to the maximal TER response. Results are represented as mean ± SD; *$p < 0.01$. (B) EC monolayers transfected with nonspecific RNA or Asef-specific siRNA were stimulated with thrombin (0.5 U/ml, 10 min) with or without HGF pretreatment (50 ng/ml, 15 min). Stress fiber formation and integrity of EC monolayer were monitored by immunofluorescence staining with Texas red–phalloidin. Paracellular gaps and disrupted intercellular contacts are marked by arrows. Bar, 10 μm. (C) Cells treated with nonspecific or Asef-specific siRNA were stimulated with thrombin (0.5 U/ml, 10 min) with or without HGF pretreatment (50 mg/ml, 15 min). Rho activation was evaluated by RhoGTP pull-down assay and normalized to total Rho content in cell lysates. Asef depletion was verified by Western blot. (D) Activation of Rho pathway was evaluated by Western blot analysis of phospho-MYPT and diphospho-MLC levels. Reprobing with β-actin antibody was used as the normalization control. Asef depletion was verified by Western blot. Bar graphs depict quantitative densitometry analysis of Western blot data; *$p < 0.05$, thrombin nonspecific RNA vs. HGF + thrombin nonspecific RNA; **$p < 0.05$, HGF + thrombin nonspecific RNA vs. si-Asef.

(Zheng, 2001; Servitja *et al.*, 2003; Welch *et al.*, 2003). Signaling mechanisms regulating Asef activity are not completely understood. Because Asef and Tiam1 may be regulated by different mechanisms, our present and previously published data suggest a certain overlap of GEFs in HGF-induced Rac1 activation but do not exclude different mechanisms of Tiam1 and Asef activation by HGF or other barrier-enhancing molecules.

This study demonstrates for the first time a major role of Asef in lung barrier protection in the two-hit animal model of acute lung injury. Absence of Asef is compatible with normal physiological functioning of mice, and we did not observe any noticeable changes in the basal levels of BAL protein or cell counts or alterations in lung histology (unpublished data). However, Asef ablation caused nearly complete inhibition of Rac1 activation in response to vascular endothelial growth factor and basic fibroblast growth factor in cells isolated from *Asef*$^{-/-}$ mice, leading to impaired cell migration and tube formation, although expression of other Rac-specific GEFs was not affected (Kawasaki *et al.*, 2011). On the other hand, our results show significant attenuation of barrier protective and antiinflammatory effects of HGF in the TRAP6/HTV model of lung injury.

Although Asef expression by the alveolar epithelial cells was not analyzed in this study, Asef expression by epithelial cells derived from other beds has been reported (Kawasaki *et al.*, 2009; Cheng *et al.*, 2013). Therefore, in experiments with global Asef knockout, we cannot exclude a potential effect of other cell types, such as alveolar type I epithelium, on the HGF-protective effects. Evaluation of a potential Asef role in control of alveolar epithelial barrier requires further investigation. On the other

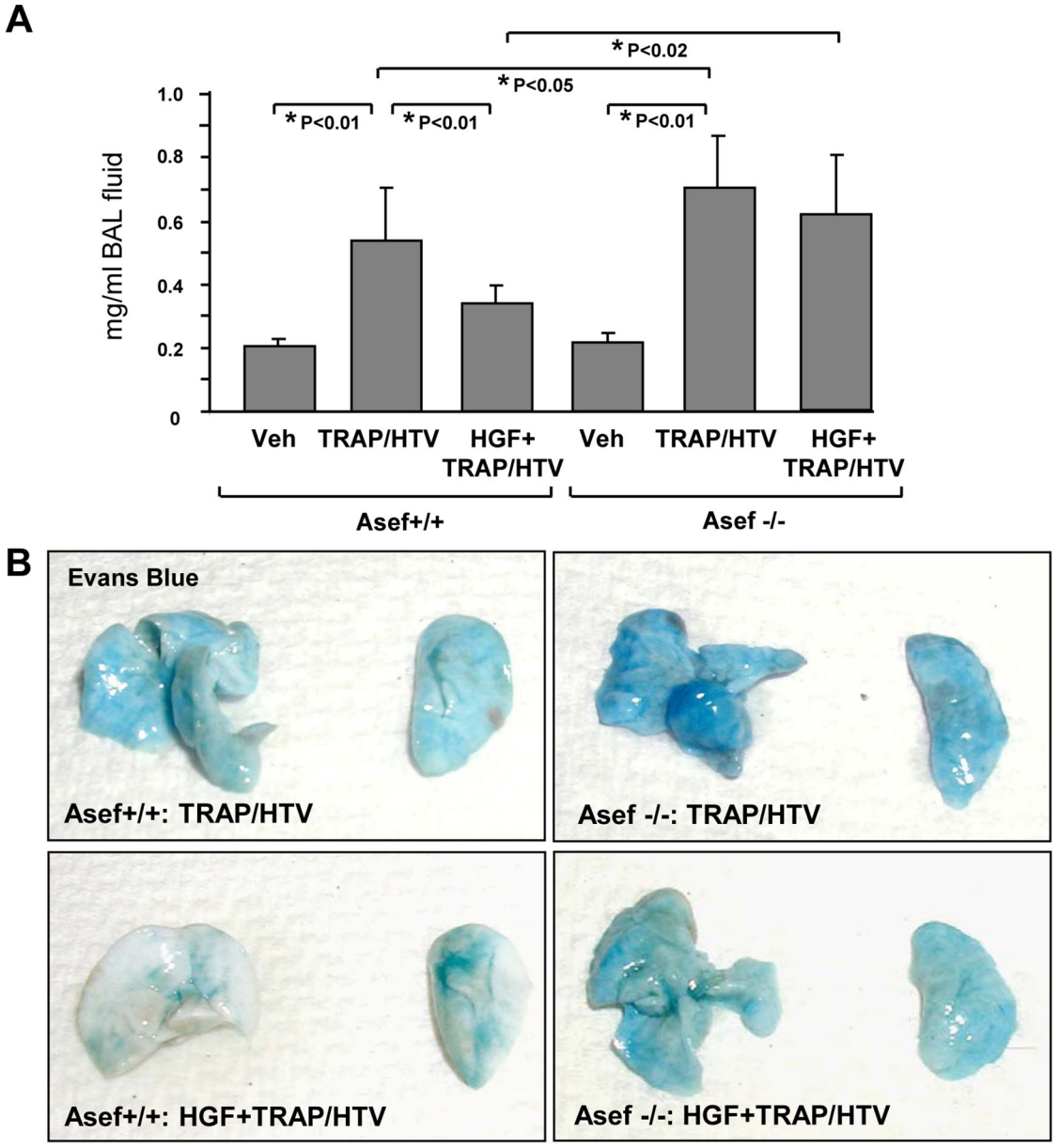
A
* P<0.02
* P<0.05
* P<0.01
* P<0.01
* P<0.01
mg/ml BAL fluid
1.0
0.8
0.6
0.4
0.2
0
Veh
TRAP/HTV
HGF+ TRAP/HTV
Veh
TRAP/HTV
HGF+ TRAP/HTV
Asef+/+
Asef -/-
B
Evans Blue
Asef+/+: TRAP/HTV
Asef -/-: TRAP/HTV
Asef+/+: HGF+TRAP/HTV
Asef -/-: HGF+TRAP/HTV
C
* P<0.05
* P<0.05
* P<0.01
Evans Blue dye, μg/g
70
60
50
40
30
20
10
0
TRAP/HTV
HGF+ TRAP/HTV
TRAP/HTV
HGF+ TRAP/HTV
Asef+/+
Asef -/-

hand, measurements of vascular permeability in vivo (Figure 8) suggest a critical involvement of lung vascular endothelium in Asef-dependent, HGF-mediated protection against ventilator-induced acute lung injury.

In summary, this study shows that HGF promotes enhancement of lung endothelial barrier properties critical for restoration of vascular barrier function. Activation of Asef-Rac–dependent lung vascular barrier restoration may represent an autoregulatory mechanism directed at down-regulation of barrier-disruptive signaling and resolution of pathological conditions. The results of this study also suggest that targeted activation of Rac1-specific GEFs such as Asef may accelerate endothelial barrier recovery and promote resolution of lung injury.

MATERIALS AND METHODS

Cell culture and reagents

HPAECs were obtained from Lonza (East Rutherford, NJ) and used for experiments at passages 5–7. Subconfluent HPAEC cultures were plated at density 260 cells/mm^2 and grown for 48 h to reach 70–80% confluence. To achieve sparse and completely confluent cell monolayers, HPAEC were plated at 150 and 600 cells/mm^2, respectively. In studies with thrombin model of endothelial disruption, the cells were grown for 72 h to reach 100% confluence (600–700 cells/mm^2). In experiments with DNA transfections, the cells were plated at 30–40% density, transfected the next day, and analyzed after 24 h of transfection. In experiments with siRNA transfections, the cells were plated at 30–40% density, transfected the next day, grown for 48 h, and then replated at lower density and analyzed after 24 h (total transfection time, 72 h). For TER measurements, the cells were grown for 72 h after transfection without replating. Plasmids encoding hemagglutinin (HA)-tagged wild-type Asef, dominant-negative AsefΔ^{DH}, and constitutively active AsefΔ^{APC} mutants subcloned into pcDNA3.1 (Invitrogen, Carlsbad, CA) were described elsewhere (Kawasaki *et al.*, 2003). Human HGF was obtained from R&D Systems (Minneapolis, MN). The cell-permeable c-Met kinase inhibitor *N*-(3-fluoro-4-(7-methoxy-4-quinolinyl)phenyl)-1-(2-hydroxy-2-methylpropyl)-5-methyl-3-oxo-phenyl-2,3-dihydro-1H-pyrazole carboxamide was purchased from Millipore (Billerica, MA). Texas red–conjugated phalloidin and Alexa Flour 488 were purchased from Molecular Probes (Eugene, OR). Asef, Rac1, RhoA, and HA-tag antibodies were purchased from Santa Cruz Biotechnology (Santa Cruz, CA); cortactin and phospho–Tyr-421 cortactin antibodies were from Millipore; and horseradish peroxidase–linked anti-mouse immunoglobulin G, di-phospho-MLC, and phospho-MYPT antibodies were obtained from Cell Signaling (Beverly, MA). Unless otherwise specified, all biochemical reagents, including β-actin antibodies, were obtained from Sigma-Aldrich (St. Louis, MO).

Asef knockdown in human pulmonary EC culture

To deplete endogenous Asef, an Asef-specific set of three Stealth Select siRNA duplexes was purchased from Invitrogen in ready-to-use, desalted, deprotected, annealed, double-strand form. Nonspecific RNA (Dharmacon, Lafayette, CO) was used as a control treatment. Transfection of ECs with siRNA was performed as previously described (Birukova *et al.*, 2010). After 72 h of transfection, cells were used for experiments or harvested for Western blot verification of specific protein depletion.

GTPase and GEF activation assays

Rac1 and RhoA activation was evaluated in pull-down assays using agarose beads with immobilized PAK1-PBD and rhotekin-RBD, respectively (Birukov *et al.*, 2004). In brief, after stimulation, cell lysates were collected, and GTP-bound Rac1 or Rho was captured using pull-down assays with immobilized PAK1-PBD or Rhotekin-RBD, respectively. The levels of activated small GTPases, as well as of total Rac1 and Rho content, were evaluated by Western blot analysis. Active Asef was affinity precipitated from cell lysates according to a previously described protocol (Waheed *et al.*, 2013) using the Rac1 (G15A) mutant that cannot bind nucleotide and therefore has high affinity for activated GEFs (Garcia-Mata *et al.*, 2006). Activated Asef in Rac1 (G15A) pull downs was detected by Western blotting and normalized to total Asef in cell lysates for each sample. Precipitation with glutathione–Sepharose beads containing no fusion proteins resulted in no Asef precipitation.

Fluorescence resonance energy transfer

The Rac1-FRET biosensor was kindly provided by Yingxiao Wang (University of Illinois, Urbana-Champaign, IL). FRET analysis was performed as described elsewhere (Poh *et al.*, 2009; Birukova *et al.*, 2012). Cells were seeded on glass-bottom dishes (MatTek, Ashland, MA) coated with gelatin. At 24 h after transfection, medium was changed to 2% fetal bovine serum endothelial basal medium (EBM) for 2 h. For detection of FRET, the cells were maintained on the microscope stage at 37°C. To minimize the photobleaching effect, the time interval for each imaging acquisition was set to be 30 s, and images were captured for 10 min using an Olympus model IX71 microscope system (Olympus, Tokyo, Japan) equipped with a 60× oil immersion objective and a charge-coupled device camera. MetaMorph software (Molecular Devices, Sunnyvale, CA) was used to control the filter wheel and data analysis. The ratiometric images of ECFP/YPet were computed and generated by the MetaMorph software to represent the spatiotemporal FRET signals. Analysis of regional Rac1 activation was performed using integral ECFP/YPet values in ~5-μm- wide areas at the cell periphery and equal areas in the central parts of the cell. Increased Rac1 activation (ECFP/YPet emission ratio) at the cell periphery was normalized to Rac1 activation in central parts of the cell and expressed as bar graphs. Comparisons were made between unstimulated cells and cells stimulated with HGF (6 min) with and without Asef depletion.

Live imaging of cells expressing GFP-cortactin

Cells were plated on MatTek dishes and transfected with GFP-cortactin. Images were acquired with 100×/numerical aperture 1.45 oil objective in a 3I Marianas Yokogawa-type spinning disk confocal system equipped with a CO_2 chamber and a heated stage. Time-lapse images were taken at 2-s intervals for 30 min.

FIGURE 8: Role of Asef in HGF-induced lung barrier protection in the model of TRAP6/HTV-induced lung injury. *Asef*$^{+/+}$ and *Asef*$^{-/-}$ mice were treated with vehicle or HGF (500 μg/kg, intravenous), followed by TRAP6 injection (1.5×10^{-5} mol/kg, intratracheal) and mechanical ventilation at high tidal volume (HTV, 30 ml/kg, 4 h). (A) Measurements of protein concentration in BAL fluid; $n = 6$. (B) Vascular leak was analyzed by Evans blue–labeled albumin extravasation into the lung tissue. (C) The quantitative analysis of Evans blue–labeled albumin extravasation was performed by spectrophotometric evaluation of Evans blue extracted from the lung tissue samples; $n = 6$.

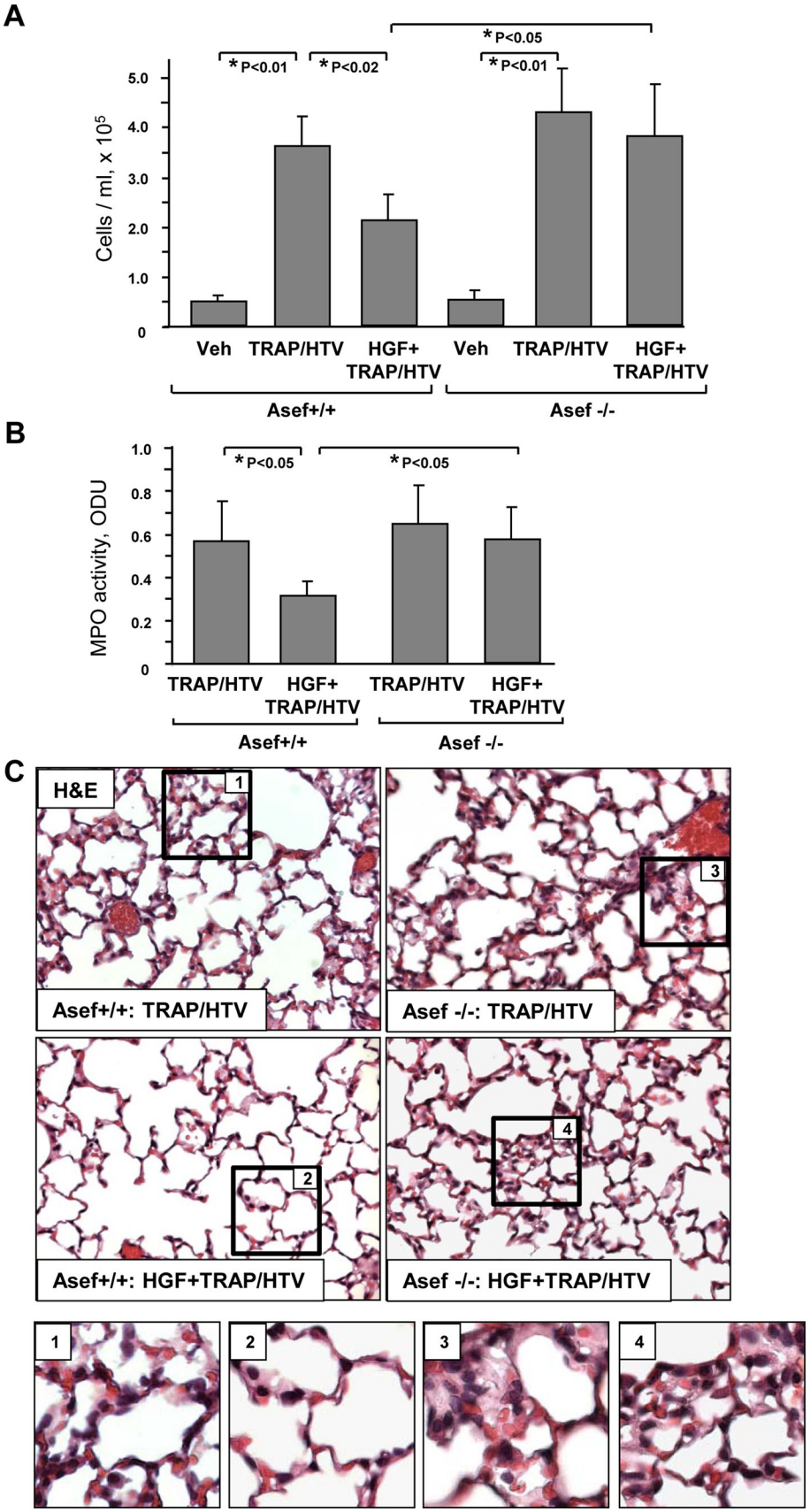

FIGURE 9: Role of Asef in the HGF protection against leukocyte infiltration in TRAP6/HTV-induced lung injury. *Asef*$^{+/+}$ and *Asef*$^{-/-}$ mice were treated with vehicle or HGF (500 μg/kg, intravenous), followed by TRAP6 injection (1.5×10^{-5} mol/kg, intratracheal) and mechanical ventilation at high tidal volume (HTV, 30 ml/kg, 4 h). (A) Total cell count and neutrophil count were performed in BAL fluid; $n = 6$. (B) Measurements of MPO activity in lung samples from *Asef*$^{+/+}$ and *Asef*$^{-/-}$ mice exposed to TRAP6/HTV with or without HGF pretreatment; $n = 4$. (C) Whole lungs were fixed in 10% Formalin and used for histological evaluation by hematoxylin and eosin staining. Images are representative of four to six lung specimens for each condition with 40× magnification. Insets, higher-magnification images of lung tissue.

Immunofluorescence

Endothelial monolayers plated on glass coverslips were treated with the agonist of interest, fixed in 3.7% formaldehyde solution in phosphate-buffered saline (PBS) for 10 min at 4°C, washed three times with PBS, permeabilized with 0.1% Triton X-100 in PBS-Tween (PBST) for 30 min at room temperature, and blocked with 2% bovine serum albumin (BSA) in PBST for 30 min. Incubation with Asef or HA-tag antibodies was performed in blocking solution (2% BSA in PBST) for 1 h at room temperature, followed by staining with Alexa 488–conjugated secondary antibodies. Actin filaments were stained with Texas red–conjugated phalloidin. After immunostaining, slides were analyzed using a Nikon video imaging system (Nikon Instech, Tokyo, Japan) as described elsewhere (Birukov *et al.*, 2004; Birukova *et al.*, 2004b).

Differential protein fractionation and immunoblotting

Confluent HPAECs were stimulated with HGF; cytosolic and membrane fractions were isolated using a subcellular protein fractionation kit (Thermo Fisher Scientific, Rockford, IL) according to manufacturer's protocol. Asef and cortactin membrane translocation was evaluated by Western blot detection of changes in protein content in equal volumes of membrane fractions obtained from control and HGF-stimulated cells. For analysis of protein phosphorylation profile, cells were stimulated and then lysed, and protein extracts were separated by SDS–PAGE, transferred to polyvinylidene fluoride membrane, and probed with specific antibodies. Equal protein loading was verified by probing of membranes with antibody to β-actin or a specific protein of interest.

Permeability measurements

Endothelial permeability to macromolecules was monitored by express permeability testing assay (XPerT) recently developed in our group (Dubrovskyi *et al.*, 2013) and now available from Millipore (Vascular Permeability Imaging Assay, catalogue #17-10398). This assay is based on high-affinity binding of cell-impermeable, avidin-conjugated,

FITC-labeled tracer to the biotinylated extracellular matrix proteins immobilized on the bottom of culture dishes covered with EC monolayers. FITC-avidin binding to the matrix-coated culture dish bottoms increases if the EC barrier is compromised by treatment with a barrier-disruptive agonist. In permeability visualization experiments, 15 min after EC stimulation with HGF, FITC-avidin solution was added directly to the culture medium for 3 min before termination of the experiment. Unbound FITC-avidin was washed out with PBS (pH 7.4, 37°C), cells were fixed with 3.7% formaldehyde in PBS (10 min, room temperature), and visualization of FITC-avidin on the bottoms of coverslips was performed using the Nikon imaging system Eclipse TE 300 equipped with a digital camera (DKC 5000; Sony, Tokyo, Japan); 10× objective lenses were used. Images were processed with Photoshop 7.0 software (Adobe Systems, San Jose, CA). Measurements of TER across confluent HPAEC monolayers were performed using the electrical cell-substrate impedance-sensing system (Applied Biophysics, Troy, NY) as previously described (Birukov *et al.*, 2004; Birukova *et al.*, 2004a).

Mechanical ventilation protocol

All experimental protocols involving the use of animals were approved by the University of Chicago Institutional Animal Care and Use Committee for the Humane Treatment of Experimental Animals. Generation of *Asef*$^{-/-}$ mice is described elsewhere (Kawasaki *et al.*, 2011). C57Bl-6J *Asef*$^{-/-}$ mice and matching controls (8- to 10-wk-old males) with average weight 20–25 g were anesthetized with an intraperitoneal injection of ketamine (75 mg/kg) and acepromazine (1.5 mg/kg) and subjected to mechanical ventilation with high tidal volume as previously described (Birukova *et al.*, 2010, 2011). Briefly, tracheotomy was performed, and the trachea was cannulated with a 20-gauge, 1-in. catheter, which was tied into place to prevent air leak. The animals were then placed on a mechanical ventilator (Harvard Apparatus, Boston, MA). Mice were randomized to concurrently receive sterile saline solution or HGF (500 µg/kg, intravenous administration) before a single dose of TRAP6 (1.5×10^{-5} mol/kg, intratracheal instillation), followed by 4 h of mechanical ventilation with high tidal volume (30 ml/kg, 75 breaths/min, and zero positive end-expiratory pressure, high tidal volume). Control animals were anesthetized and allowed to breathe spontaneously.

Evaluation of lung injury parameters

After the experiment, BAL was performed using 1 ml of sterile Hank's balanced saline buffer. The BAL protein concentration was determined by BCATM Protein Assay kit (Thermo Scientific, Pittsburgh, PA). BAL inflammatory cell counting was performed using a standard hemacytometer technique (Birukova *et al.*, 2007b; Fu *et al.*, 2009). Total lung MPO content was determined from homogenized lungs as described elsewhere (Meliton *et al.*, 2013). For analysis of TRAP6/HTV-induced lung vascular leak, Evans blue dye (30 ml/kg) was injected into the external jugular vein 2 h before termination of the experiment. Measurement of Evans blue accumulation in the lung tissue was performed by spectrofluorimetric analysis of lung tissue lysates according to a protocol described previously (Moitra *et al.*, 2007; Nonas *et al.*, 2008). For histological assessment of lung injury, the lungs were harvested without lavage collection and fixed in 10% formaldehyde. After fixation, the lungs were embedded in paraffin, cut into 5-µm sections, and stained with hematoxylin and eosin. Sections were evaluated at 40× magnification.

Statistical analysis

Results are expressed as mean ± SD of three to six independent experiments. Stimulated samples were compared with controls by unpaired Student's *t* tests. For multiple-group comparisons, a two-way analysis of variance followed by a Tukey posthoc test was used. $p < 0.05$ was considered statistically significant.

ACKNOWLEDGMENTS

We thank Katalin Szaszi (St. Michael's Hospital, Toronto, Canada) for sharing the RacG15A construct. This work was supported by grants from the National Heart, Lung, and Blood Institute (HL89257 and HL107920) to A.B. and Grants-in-Aid for Scientific Research on Innovative Areas (Integrative Research on Cancer Microenvironment Network), Ministry of Education, Culture, Sports, Science and Technology, Japan, to T.A.

REFERENCES

Acute Respiratory Distress Syndrome Network (2000). Ventilation with lower tidal volumes as compared with traditional tidal volumes for acute lung injury and the acute respiratory distress syndrome. N Engl J Med 342, 1301–1308.

Ammer AG, Weed SA (2008). Cortactin branches out: roles in regulating protrusive actin dynamics. Cell Motil Cytoskeleton 65, 687–707.

Anastasiadis PZ, Moon SY, Thoreson MA, Mariner DJ, Crawford HC, Zheng Y, Reynolds AB (2000). Inhibition of RhoA by p120 catenin. Nat Cell Biol 2, 637–644.

Arthur WT, Noren NK, Burridge K (2002). Regulation of Rho family GTPases by cell-cell and cell-matrix adhesion. Biol Res 35, 239–246.

Baumer Y, Spindler V, Werthmann RC, Bunemann M, Waschke J (2009). Role of Rac 1 and cAMP in endothelial barrier stabilization and thrombin-induced barrier breakdown. J Cell Physiol 220, 716–726.

Birukov KG, Bochkov VN, Birukova AA, Kawkitinarong K, Rios A, Leitner A, Verin AD, Bokoch GM, Leitinger N, Garcia JG (2004). Epoxycyclopentenone-containing oxidized phospholipids restore endothelial barrier function via Cdc42 and Rac. Circ Res 95, 892–901.

Birukov KG, Zebda N, Birukova AA (2013). Barrier enhancing signals in pulmonary edema. Compr Physiol 3, 429–484.

Birukova AA, Alekseeva E, Mikaelyan A, Birukov KG (2007a). HGF attenuates thrombin-induced permeability in the human pulmonary endothelial cells by Tiam1-mediated activation of the Rac pathway and by Tiam1/Rac-dependent inhibition of the Rho pathway. FASEB J 21, 2776–2786.

Birukova AA, Birukov KG, Smurova K, Adyshev DM, Kaibuchi K, Alieva I, Garcia JG, Verin AD (2004a). Novel role of microtubules in thrombin-induced endothelial barrier dysfunction. FASEB J 18, 1879–1890.

Birukova AA, Fu P, Chatchavalvanich S, Burdette D, Oskolkova O, Bochkov VN, Birukov KG (2007b)). Polar head groups are important for barrier protective effects of oxidized phospholipids on pulmonary endothelium. Am J Physiol Lung Cell Mol Physiol 292, L924–L935.

Birukova AA, Fu P, Xing J, Yakubov B, Cokic I, Birukov KG (2010). Mechanotransduction by GEF-H1 as a novel mechanism of ventilator-induced vascular endothelial permeability. Am J Physiol Lung Cell Mol Physiol 298, L837–L848.

Birukova AA, Smurova K, Birukov KG, Kaibuchi K, Garcia JGN, Verin AD (2004b). Role of Rho GTPases in thrombin-induced lung vascular endothelial cells barrier dysfunction. Microvasc Res 67, 64–77.

Birukova AA, Tian Y, Dubrovskyi O, Zebda N, Sarich N, Tian X, Wang Y, Birukov KG (2012). VE-cadherin trans-interactions modulate Rac activation and enhancement of lung endothelial barrier by iloprost. J Cell Physiol 227, 3405–3416.

Birukova AA, Zagranichnaya T, Alekseeva E, Fu P, Chen W, Jacobson JR, Birukov KG (2007c). Prostaglandins PGE2 and PGI2 promote endothelial barrier enhancement via PKA- and Epac1/Rap1-dependent Rac activation. Exp Cell Res 313, 2504–2520.

Birukova AA, Zebda N, Cokic I, Fu P, Wu T, Dubrovskyi O, Birukov KG (2011). p190RhoGAP mediates protective effects of oxidized phospholipids in the models of ventilator-induced lung injury. Exp Cell Res 317, 859–872.

Bishop AL, Hall A (2000). Rho GTPases and their effector proteins. Biochem J 348, 241–255.

Blank R, Napolitano LM (2011). Epidemiology of ARDS and ALI. Crit Care Clin 27, 439–458.

Boguski MS, McCormick F (1993). Proteins regulating Ras and its relatives. Nature 366, 643–654.

Borisy GG, Svitkina TM (2000). Actin machinery: pushing the envelope. Curr Opin Cell Biol 12, 104–112.
Cheng HT, Juang IP, Chen LC, Lin LY, Chao CH (2013). Association of Asef and Cdc42 expression to tubular injury in diseased human kidney. J Invest Med 61, 1097–1103.
Dubrovskyi O, Birukova AA, Birukov KG (2013). Measurement of local permeability at subcellular level in cell models of agonist- and ventilator-induced lung injury. Lab Invest 93, 254–263.
Dudek SM, Jacobson JR, Chiang ET, Birukov KG, Wang P, Zhan X, Garcia JG (2004). Pulmonary endothelial cell barrier enhancement by sphingosine 1-phosphate: roles for cortactin and myosin light chain kinase. J Biol Chem 279, 24692–24700.
Essler M, Amano M, Kruse HJ, Kaibuchi K, Weber PC, Aepfelbacher M (1998). Thrombin inactivates myosin light chain phosphatase via Rho and its target Rho kinase in human endothelial cells. J Biol Chem 273, 21867–21874.
Finigan JH, Dudek SM, Singleton PA, Chiang ET, Jacobson JR, Camp SM, Ye SQ, Garcia JG (2005). Activated protein C mediates novel lung endothelial barrier enhancement: role of sphingosine 1-phosphate receptor transactivation. J Biol Chem 280, 17286–17293.
Fu P, Birukova AA, Xing J, Sammani S, Murley JS, Garcia JG, Grdina DJ, Birukov KG (2009). Amifostine reduces lung vascular permeability via suppression of inflammatory signalling. Eur Respir J 33, 612–624.
Fukuhara S, Sakurai A, Sano H, Yamagishi A, Somekawa S, Takakura N, Saito Y, Kangawa K, Mochizuki N (2005). Cyclic AMP potentiates vascular endothelial cadherin-mediated cell-cell contact to enhance endothelial barrier function through an Epac-Rap1 signaling pathway. Mol Cell Biol 25, 136–146.
Garcia-Mata R, Wennerberg K, Arthur WT, Noren NK, Ellerbroek SM, Burridge K (2006). Analysis of activated GAPs and GEFs in cell lysates. Methods Enzymol 406, 425–437.
Garcia JG, Liu F, Verin AD, Birukova A, Dechert MA, Gerthoffer WT, Bamberg JR, English D (2001). Sphingosine 1-phosphate promotes endothelial cell barrier integrity by Edg-dependent cytoskeletal rearrangement. J Clin Invest 108, 689–701.
Geiser T (2003). Mechanisms of alveolar epithelial repair in acute lung injury—a translational approach. Swiss Med Wkly 133, 586–590.
Head JA, Jiang D, Li M, Zorn LJ, Schaefer EM, Parsons JT, Weed SA (2003). Cortactin tyrosine phosphorylation requires Rac1 activity and association with the cortical actin cytoskeleton. Mol Biol Cell 14, 3216–3229.
Kawasaki Y, Furukawa S, Sato R, Akiyama T (2013). Differences in the localization of the adenomatous polyposis coli-Asef/Asef2 complex between adenomatous polyposis coli wild-type and mutant cells. Cancer Sci 104, 1135–1138.
Kawasaki Y, Jigami T, Furukawa S, Sagara M, Echizen K, Shibata Y, Sato R, Akiyama T (2011). The adenomatous polyposis coli-associated guanine nucleotide exchange factor Asef is involved in angiogenesis. J Biol Chem 285, 1199–1207.
Kawasaki Y, Sato R, Akiyama T (2003). Mutated APC and Asef are involved in the migration of colorectal tumour cells. Nat Cell Biol 5, 211–215.
Kawasaki Y, Senda T, Ishidate T, Koyama R, Morishita T, Iwayama Y, Higuchi O, Akiyama T (2000). Asef, a link between the tumor suppressor APC and G-protein signaling. Science 289, 1194–1197.
Kawasaki Y, Tsuji S, Sagara M, Echizen K, Shibata Y, Akiyama T (2009). Adenomatous polyposis coli and Asef function downstream of hepatocyte growth factor and phosphatidylinositol 3-kinase. J Biol Chem 284, 22436–22443.
Liu F, Schaphorst KL, Verin AD, Jacobs K, Birukova A, Day RM, Bogatcheva N, Bottaro DP, Garcia JG (2002). Hepatocyte growth factor enhances endothelial cell barrier function and cortical cytoskeletal rearrangement: potential role of glycogen synthase kinase-3beta. FASEB J 16, 950–962.
Matsumoto K, Nakamura T (1996). Emerging multipotent aspects of hepatocyte growth factor. J Biochem 119, 591–600.
Matthay MA, Zimmerman GA, Esmon C, Bhattacharya J, Coller B, Doerschuk CM, Floros J, Gimbrone MA Jr, Hoffman E, Hubmayr RD, *et al.* (2003). Future research directions in acute lung injury: summary of a National Heart, Lung, and Blood Institute working group. Am J Respir Crit Care Med 167, 1027–1035.
Meliton AY, Munoz NM, Meliton LN, Birukova AA, Leff AR, Birukov KG (2013). Mechanical induction of group V phospholipase A(2) causes lung inflammation and acute lung injury. Am J Physiol Lung Cell Mol Physiol 304, L689–L700.
Moitra J, Sammani S, Garcia JG (2007). Re-evaluation of Evans Blue dye as a marker of albumin clearance in murine models of acute lung injury. Transl Res 150, 253–265.
Nimnual AS, Taylor LJ, Bar-Sagi D (2003). Redox-dependent downregulation of Rho by Rac. Nat Cell Biol 5, 236–241.
Nonas S, Birukova AA, Fu P, Xing J, Chatchavalvanich S, Bochkov VN, Leitinger N, Garcia JG, Birukov KG (2008). Oxidized phospholipids reduce ventilator-induced vascular leak and inflammation in vivo. Crit Care 12, R27.
Noren NK, Niessen CM, Gumbiner BM, Burridge K (2001). Cadherin engagement regulates Rho family GTPases. J Biol Chem 276, 33305–33308.
Poh YC, Na S, Chowdhury F, Ouyang M, Wang Y, Wang N (2009). Rapid activation of Rac GTPase in living cells by force is independent of Src. PLoS One 4, e7886.
Quesnel C, Marchand-Adam S, Fabre A, Marchal-Somme J, Philip I, Lasocki S, Lecon V, Crestani B, Dehoux M (2008). Regulation of hepatocyte growth factor secretion by fibroblasts in patients with acute lung injury. Am J Physiol Lung Cell Mol Physiol 294, L334–L343.
Servitja JM, Marinissen MJ, Sodhi A, Bustelo XR, Gutkind JS (2003). Rac1 function is required for Src-induced transformation. Evidence of a role for Tiam1 and Vav2 in Rac activation by Src. J Biol Chem 278, 34339–34346.
Singleton PA, Salgia R, Moreno-Vinasco L, Moitra J, Sammani S, Mirzapoiazova T, Garcia JG (2007). CD44 regulates hepatocyte growth factor-mediated vascular integrity. Role of c-Met, Tiam1/Rac1, dynamin 2, and cortactin. J Biol Chem 282, 30643–30657.
Stern JB, Fierobe L, Paugam C, Rolland C, Dehoux M, Petiet A, Dombret MC, Mantz J, Aubier M, Crestani B (2000). Keratinocyte growth factor and hepatocyte growth factor in bronchoalveolar lavage fluid in acute respiratory distress syndrome patients. Crit Care Med 28, 2326–2333.
Storck J, Zimmermann ER (1996). Regulation of the thrombin receptor response in human endothelial cells. Thromb Res 81, 121–131.
Stultiens A, Ho TT, Nusgens BV, Colige AC, Deroanne CF (2012). Rho proteins crosstalk via RhoGDIalpha: at random or hierarchically ordered? Commun Integr Biol 5, 99–101.
Tauseef M, Kini V, Knezevic N, Brannan M, Ramchandaran R, Fyrst H, Saba J, Vogel SM, Malik AB, Mehta D (2008). Activation of sphingosine kinase-1 reverses the increase in lung vascular permeability through sphingosine-1-phosphate receptor signaling in endothelial cells. Circ Res 103, 1164–1172.
Tian Y, Tian X, Gawlak G, O'Donnell JJ 3rd, Sacks DB, Birukova AA (2014). IQGAP1 regulates endothelial barrier function via EB1-cortactin cross-talk. Mol Cell Biol 34, 3546–3558.
Uruno T, Liu J, Zhang P, Fan Y, Egile C, Li R, Mueller SC, Zhan X (2001). Activation of Arp2/3 complex-mediated actin polymerization by cortactin. Nat Cell Biol 3, 259–266.
Velasco G, Armstrong C, Morrice N, Frame S, Cohen P (2002). Phosphorylation of the regulatory subunit of smooth muscle protein phosphatase 1M at Thr850 induces its dissociation from myosin. FEBS Lett 527, 101–104.
Verghese GM, McCormick-Shannon K, Mason RJ, Matthay MA (1998). Hepatocyte growth factor and keratinocyte growth factor in the pulmonary edema fluid of patients with acute lung injury. Biologic and clinical significance. Am J Respir Crit Care Med 158, 386–394.
Vouret-Craviari V, Bourcier C, Boulter E, van Obberghen-Schilling E (2002). Distinct signals via Rho GTPases and Src drive shape changes by thrombin and sphingosine-1-phosphate in endothelial cells. J Cell Sci 115, 2475–2484.
Waheed F, Dan Q, Amoozadeh Y, Zhang Y, Tanimura S, Speight P, Kapus A, Szaszi K (2013). Central role of the exchange factor GEF-H1 in TNF-alpha-induced sequential activation of Rac, ADAM17/TACE, and RhoA in tubular epithelial cells. Mol Biol Cell 24, 1068–1082.
Ware LB, Matthay MA (2002). Keratinocyte and hepatocyte growth factors in the lung: roles in lung development, inflammation, and repair. Am J Physiol Lung Cell Mol Physiol 282, L924–L940.
Weed SA, Du Y, Parsons JT (1998). Translocation of cortactin to the cell periphery is mediated by the small GTPase Rac1. J Cell Sci 111, 2433–2443.
Weed SA, Parsons JT (2001). Cortactin: coupling membrane dynamics to cortical actin assembly. Oncogene 20, 6418–6434.
Welch HC, Coadwell WJ, Stephens LR, Hawkins PT (2003). Phosphoinositide 3-kinase-dependent activation of Rac. FEBS Lett 546, 93–97.
Zebda N, Tian Y, Tian X, Gawlak G, Higginbotham K, Reynolds AB, Birukova AA, Birukov KG (2013). Interaction of p190RhoGAP with C-terminal domain of p120-catenin modulates endothelial cytoskeleton and permeability. J Biol Chem 288, 18290–18299.
Zheng Y (2001). Dbl family guanine nucleotide exchange factors. Trends Biochem Sci 26, 724–732.